ACS APPLIED OPTICAL MATERIALS

pubs.acs.org/acsaom

Forum Article

Influence of Chromophore Packing on Multiphoton Absorption in Carbazole-Based Pillar-Layered Coordination Polymers

Simon N. Deger,[⊥] Yang Cui,[⊥] Julien Warnan, Roland A. Fischer, František Šanda, Jürgen Hauer,* and Alexander Pöthig*

Cite This: *ACS Appl. Opt. Mater.* 2024, 2, 1770−1779

Read Online

ACCESS | Metrics & More | Article Recommendations | Supporting Information

ABSTRACT: Coordination polymers (CP) and their subgroup metal−organic frameworks (MOF) are promising classes of modular multiphoton-absorption active materials. However, a detailed knowledge of the structure−property relationship or generalized design principles remains elusive. This study examines how various packings of the chromophore linker 9,9′-stilbene-bis-carbazole-3,6-dicarboxylic acid in three synthesized zinc-based CPs affect their MPA activity. Different spatial chromophore arrangements are achieved by the so-called "pillar-layer" synthesis approach, using the chromophore and two different additional pillar linkers (4,4′-bipyridine and 1,2-bis(4-pyridyl)ethane) for CP formation. Two novel pillar-layered CPs, $Zn_{2n}(sbcd)(bpy)(DMAc)_{2n}(H_2O)_{3n}$ and $Zn_{2n}(sbcd)(bpe)(DMAc)_{3n}(H_2O)$, are reported and examined in their two-photon-absorption-induced photoluminescence and compared to a previously synthesized CP $Zn_{2n}(sbcd)(DMAc)_{2n}(H_2O)_{1.5n}$, containing the same chromophore but no pillars. The comparison shows significant differences for the two-photon absorption cross-sections of the materials, improving it by incorporating the pillar. Our findings point toward the significance of controlling the chromophore orientation to tailor the nonlinear optical properties of the materials. These insights pave the way toward an aim-directed development of MOFs for advanced photonic applications.

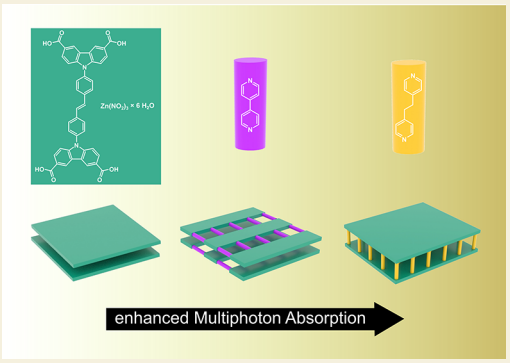

KEYWORDS: *coordination polymers, metal−organic frameworks, multiphoton absorption, nonlinear optics, structure−property relationships, single crystals*

INTRODUCTION

The invention of lasers has been a transformative milestone in scientific research, enabling significant advances across various disciplines.[1] Among the previously inaccessible optical phenomena, triplet−triplet up-conversion[2] and nonlinear optical (NLO) effects have gained prominence. NLO effects and materials are currently being explored for their application in optical filters and information encryption.[3−5] One of the best studied NLO effects is multiphoton absorption (MPA), having found applications in bioimaging,[6] 3D-data storage,[7] and other implementations.[8] MPA belongs to the group of third-order NLO processes, as it involves the conversion from a lower energy level to a higher energy level through simultaneous absorption of multiple photons in a single event.[8−10] The fundamental effect is, therefore, two-photon absorption (2PA), which is quantified by the two-photon absorption cross-section ($\sigma^{(2)}$), measured using the Göppert−Mayer unit (GM = 10^{-50} cm^4 × s × photon^{-1}).[11]

The fundamental difference between one photon absorption (1PA) and 2PA becomes obvious in the expressions for the transition moments $M_{fg}^{(1),(2)}$ between the ground (g) and excited states (f), where the superscript in parentheses stands for 1PA or 2PA, respectively.[12] The respective absorption cross-sections scale with the expectation value of $|M_{fg}^{(1),(2)}|^2$. For 1PA the matrix elements is:

$$M_{fg}^{(1)} = \langle f|\vec{E}\cdot\vec{\mu}|g\rangle \quad (1)$$

where $\vec{E}$ stands for the excitation light field along a defined polarization direction and $\vec{\mu}$ is the dipole moment operator. Two-photon absorption is most efficient if the frequency of the driving laser ω_L meets a resonance condition given by $\omega_{f'g} = 2\omega_L$, where state f' is the final state reached by the 2PA process. The 2PA probability is defined by the cross-section $\sigma^{(2)} \propto |M_{f'g}^{(2)}|^2$ derived from the two-photon transition matrix element:

Special Issue: Upconversion Optical Materials

Received: February 16, 2024
Revised: March 28, 2024
Accepted: March 28, 2024
Published: April 9, 2024

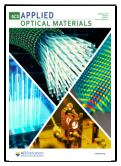

https://doi.org/10.1021/acsaom.4c00080
ACS Appl. Opt. Mater. 2024, 2, 1770−1779

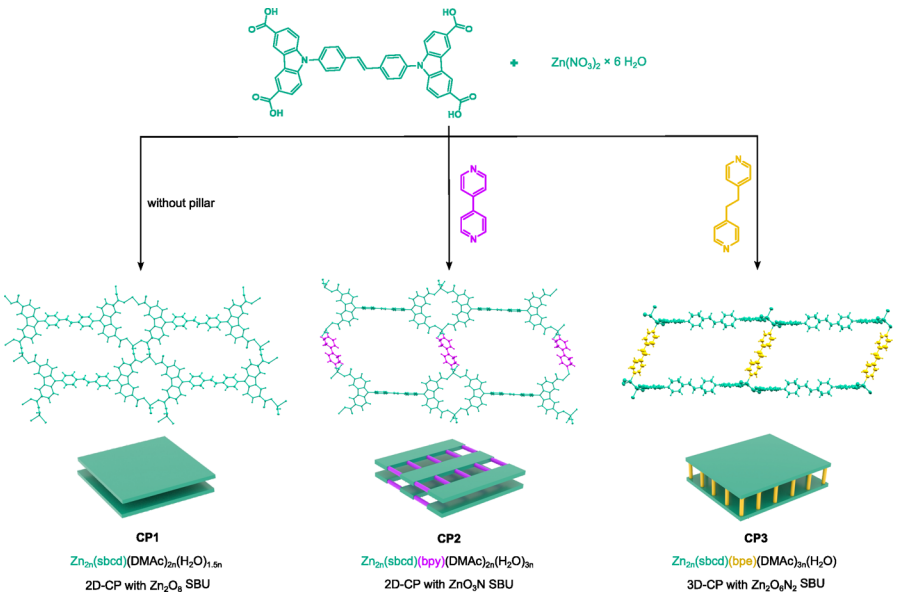

Figure 1. Overview of the synthesized materials discussed in this publication.

$$M^{(2)}_{f'g} = \frac{1}{\hbar}\sum_{e}\frac{\langle f'|\vec{E}\cdot\vec{\mu}|e\rangle\langle e|\vec{E}\cdot\vec{\mu}|g\rangle}{\omega_{eg}-\omega_{L}} \quad (2)$$

where ω_L stands for the frequency of the driving laser field and ω_{eg} for the transition frequency between the ground state and nonresonant intermediate transient levels e. The final excited state f' after 2PA is usually different from f after 1PA as the analysis of eqs 1 and 2 suggests different selection rules for them. Consequently, the transition between the ground and final state does not have to be one-photon allowed. The dependence of $M^{(2)}_{f'g}$ on detuning $\omega_{eg} - \omega_L$ is an important feature of eq 2, as only those transient e levels close to resonance with ω_L will contribute significantly.

In the search for optimized $\sigma^{(2)}$ values, different materials such as perovskites,[13] polymers,[7] and molecular organic chromophores have been investigated.[14] Organic chromophores possess the advantage of abundancy of synthesis and the potential for tuning 2PA properties by incorporating different functional groups.[15] Thereby, they access dipolar, quadrupolar, or branched molecules for increasing intermolecular interactions and consequently $\sigma^{(2)}$.[10,15] However, they possess different disadvantages, such as the tendency to aggregate and quench fluorescence in highly concentrated solutions, as well as limited optical stability.[9,11] Therefore, the stabilization of chromophores has gained research momentum, and inorganic−organic hybrid materials have been targeted as possible supporting scaffolds for chromophores.[9,11,16] In this regard, coordination polymers (CPs) and metal−organic frameworks (MOFs) are promising modular materials from their abundant organic linkers spatially templated by secondary building units (SBUs), predominantly metal-oxo clusters.[17] They are known to have a wide variety of potential applications, e.g., catalysis[18] or gas storage,[19] and more recently, photophysical applications like MPA.[9,11,20]

Incorporating the MPA-active chromophores into the framework has two potential immediate benefits: reducing photobleaching and enhancing the MPA cross-section.[9,21] Because of ordered crystalline structures in CPs/MOFs, ligand molecules can be fixed periodically with a controllable intermolecular distance. Therefore, dense chromophore packing may be achieved with a reduced reabsorption effect. Alternatively, a planar conformation of chromophore scaffold improves charge delocalization across molecules due to a larger overlap of π orbitals, which has proved to be a key factor that leads to optimized multiphoton absorption.[22,23] Furthermore, the rigidity of the framework can effectively limit radiationless decay pathways, which can lead to an increase in $\sigma^{(2)}$.[11,24] Additionally, the diversity in the choice of SBUs and coordination number allows for modulation of (stronger) intermolecular interaction.[25] Notably, the choice of SBUs not only influences the structural aspects but also introduces polarization effects, which facilitate the emergence of new charge transfer channels, consequently impacting the MPA cross-section.[26]

In general, pillar-layered MOFs offer the possibility of modifying the structure of MOFs without altering the (chromophore) linkers or SBUs. Via the introduction of "pillar" (linker) molecules, various aspects such as interlinker distances, pore size, and other structural features can be varied,[27] and examples of pillared-layer MOFs have been previously synthesized and investigated toward MPA activity.[28−31] However, due to the complex interplay of influencing parameters (e.g., chromophore-packing, -orientation, and -density) and challenges toward selectively synthesizing isostructural, (non)polymorphous MOFs, no general design principle for structure−property relationships in MPA active MOFs has been established.[26,30,31]

In this Article, we present the synthesis of two new pillar-layered Zn-CPs $Zn_{2n}(sbcd)(bpy)(DMAc)_{2n}(H_2O)_{3n}$ (**CP2**) and $Zn_{2n}(sbcd)(bpe)(DMAc)_{3n}(H_2O)$ (**CP3**) using the linker H_4sbcd (H_4sbcd = 9,9′-stilbene-bis-carbazole-3,6-dicarboxylic acid) with identical metals in the SBUs and chromophore linkers, differing only in the chemical structure of the incorporated "pillars", which are 4,4′-bipyridine (bpy) and 1,2-bis(4-pyridyl)ethane (bpe). This allows for the investigation of a potential structure−property relationship (between the chromophore packing and their NLO properties). The results are compared with the corresponding, pristine two-dimensional (pillar-free) Zn-CP structure $Zn_{2n}(sbcd)(DMAc)_{2n}(H_2O)_{1.5n}$ (**CP1**), previously published

https://doi.org/10.1021/acsaom.4c00080
ACS Appl. Opt. Mater. 2024, 2, 1770−1779

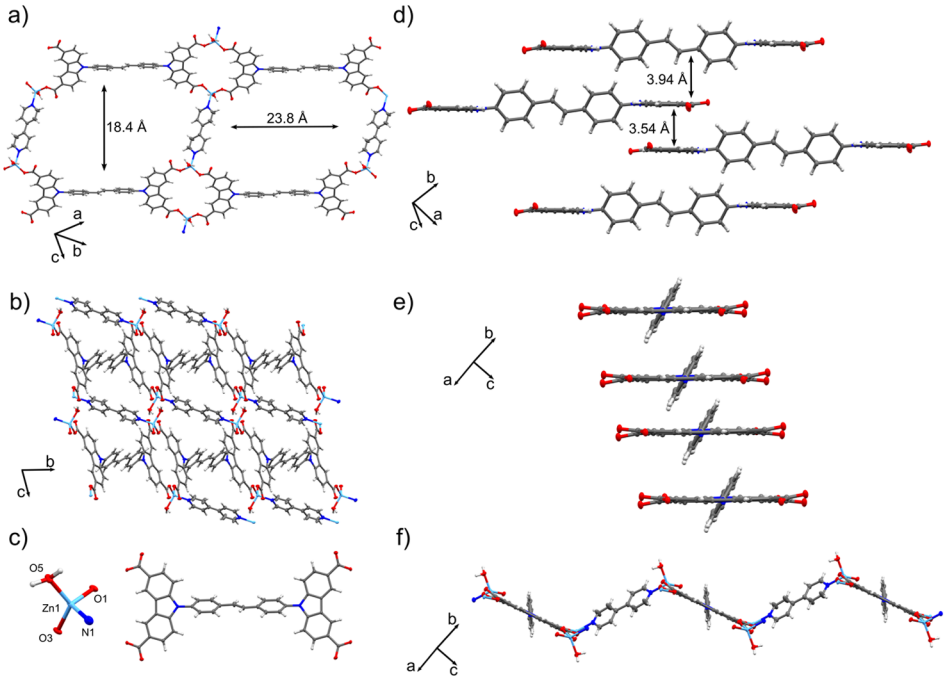

Figure 2. (a) Top view on a monolayer of **CP2** showing the interlinker and interpillar distances measured from the closest point. (b) Depiction of **CP2** along the *a* axis. (c) SBU and linker conformation inside the framework. (d) Representation of the packing and distances between the chromophores in **CP2**. (e) Visualization of the offset between the single linker strings alongside the linker N−N axis. (f) Zigzag conformation of the single CP sheets. Color coding: gray = carbon, blue = nitrogen, red = oxygen, and turquoise = zinc.

by our research group (Figure 1),[26] for which no direct structure−NLO−property relationship could be established. Compared to those of the nonpillar-layered **CP1**, the obtained data for **CP2** and **CP3** show the increase of $\sigma^{(2)}$. This indicates that the pillar-layering approach is a potential avenue to get a more comprehensive understanding of the effects of structural changes on the MOF's NLO properties and control as well as improve them.

RESULTS AND DISCUSSION

Synthesis, Structural Analysis and Comparison between $Zn_{2n}(sbcd)(DMAc)_{2n}(H_2O)_{1.5n}$ (CP1), $Zn_{2n}(sbcd)(bpy)(DMAc)_{2n}(H_2O)_{3n}$ (CP2), and $Zn_{2n}(sbcd)(bpe)(DMAc)_{3n}(H_2O)$ (CP3)

The linker molecule 9,9′-stilbene-bis-carbazole-3,6-dicarboxylic acid (H_4sbcd) was synthesized according to the previously published procedure; further information can be found in the Supporting Information (Figures S1−S3).[26] The "pillar-free" $Zn_{2n}(sbcd)(DMAc)_{2n}(H_2O)_{1.5n}$ **CP1** serves as a comparison in this study, so the influence of the pillars on packing and subsequently $\sigma^{(2)}$ of the materials can be investigated. In **CP1**, two carboxylic acid group atoms connect two zinc centers, forming a Zn_2O_8 cluster as the SBU. This SBU includes two water molecules on top of each tetrahedron. The SBUs further connect four linker molecules, leading to a 2D sheet-like sql-network topology. Alongside the *b*/*c* and *a*/*b* planes, an offset parallel stacking of the layers is observed, as expected for electron-rich-aromatic molecules, leading to an alternating packing of carbazoles and carbazole with the stilbene core.[32] In the *a*/*b* plane, a distance of 3.39 Å between the carbazoles and a carbazole−stilbene distance of 3.83 Å becomes apparent, resulting in a chromophore density of 1.40 mol/dm^3.

The CPs were synthesized by a solvothermal synthesis adjusted from that of the previously published Zn-CP (**CP1**) without the pillar.[26] To obtain phase pure and sufficiently large crystallites of the new CPs for SC-XRD analysis, the synthesis of CP1 was slightly modified. The reaction of H_4sbcd with 2.50 equiv of bpy and 3.00 equiv of $Zn(NO_3)_2{\cdot}6H_2O$ in 2.50 mL of a dimethylacetamide (DMAc)/H_2O mixture at 90 °C afforded block-shaped clear colorless single crystals which were analyzed by SC-XRD, PXRD, TGA, and IR, revealing and confirming the composition $Zn_{2n}(sbcd)(bpy)(DMAc)_{2n}(H_2O)_{3n}$ (**CP2**) as well as successful incorporation of the linker (see Figures S4−S6).

CP2 forms a two-dimensional, sheet-like framework and crystallizes in the triclinic space group $P\bar{1}$ with the unit cell parameters a = 9.8240(7) Å, b = 11.3596(8) Å, c = 13.6356(11) Å, α = 76.524(3)°, β = 73.942(3)°, and γ = 74.063(3)° (Figure 2). The sheets of the CP are composed of linker molecules arranged in strings (see Figure 2a), which are connected via the ZnO_3N SBU (see Figure 2c). The SBU is formed by two κ^1-binding linkers (O1, O3), as well as additional coordinated water, and bpy molecules, which bridge the linker strings within the sheet structure (see Figure 2c). The sheets are not planar but show a zigzag conformation (Figure 2f), exhibiting a 65.8° angle between the pillars and the linkers. They are densely packed (with a chromophore density of 1.20 mol/dm^3), held together through π stacking, and further stabilized by hydrogen bonds between the water molecules coordinated with the SBU and the uncoordinated oxygen atoms of the carboxylic acid groups of the linkers (refer to Figure 2b). The conformation of the linker inside the framework holds a 58.9° twist between the carbazole and the stilbene moiety (Figure 2c).

https://doi.org/10.1021/acsaom.4c00080
ACS Appl. Opt. Mater. 2024, 2, 1770−1779

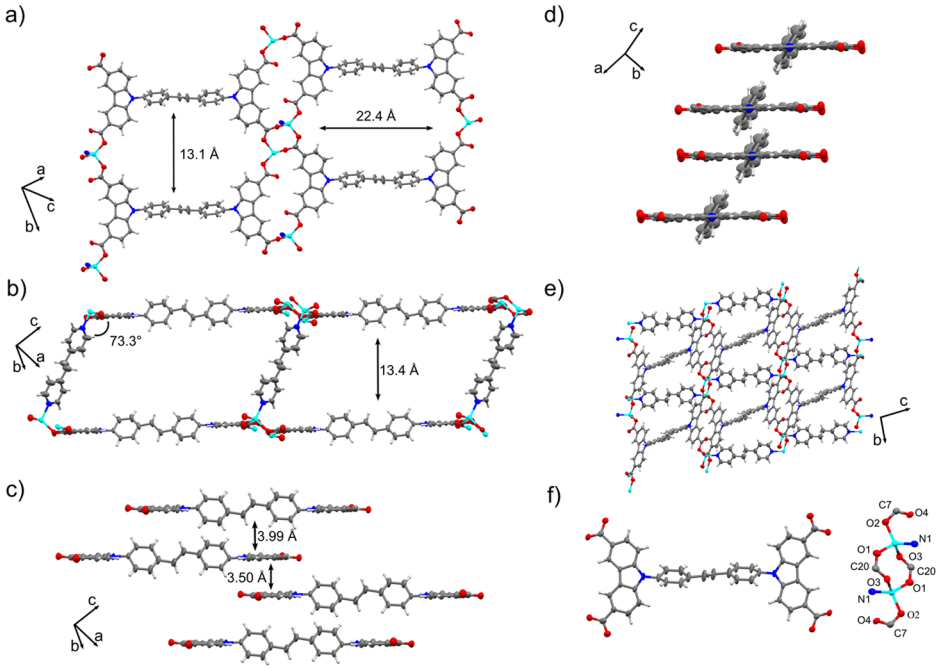

Figure 3. (a) Monolayer of the sbcd linker two-dimensional sheets in **CP3** ("linker sheets"). (b) Connection of the planar linker sheets by bpe pillars. (c) Intermolecular distances of sbcd linkers visualizing their tight packing inside the network. (d) Visualization of the offset between the single linkers alongside the linker N−N axis in the packing of **CP3**. (e) Depiction of **CP3** along the *a* axis. (f) Linker conformation inside the network and $Zn_2O_6N_2$ metal node. Color coding: gray = carbon, blue = nitrogen, red = oxygen, and turquoise = zinc.

Despite the zigzag conformation of the pillars, the linkers are stacked parallel to one another at a distance of 3.54 Å, alternating between two stacked off-center carbazoles and the built-in stilbene core, which is stacked 3.94 Å from the following carbazole (see Figure 2d). The single linker strings are shifted by 1.26 Å in relation to each other (see Figure 2e), resulting in an off-center parallel stacking, as in **CP1**.

In **CP2**, a different type of 2D periodic sheet can be observed compared to **CP1**. The bpy pillar is part of the sheet ("linker-pillar sheets") for **CP2**. The pristine dinuclear Zn_2O_8 SBU of **CP1** can be imagined to be virtually split by introduction of the bpy pillar, leading to two mononuclear Zn-SBUs bridged by bpy. This quasiextension of the SBU leads to a significant enlargement of the mesh in the 2D sheet with 13.1 × 22.4 Å compared to 18.4 × 23.8 Å for **CP1** and **CP2**, respectively.

To obtain a structurally different framework, the reaction of H_4sbcd with 3.00 equiv of $Zn(NO_3)_2{\cdot}6H_2O$ and 2.50 equiv of bpe in 2.00 mL of DMAc at 90 °C was performed. Clear block-shaped single crystals of **CP3** were obtained, crystallizing in space group $P\bar{1}$ as a three-dimensional CP. This 3D-CP consists of linker sheets assembled from the SBU and linkers as in **CP1** that are connected by the bpe pillars. A crystal has the following cell parameters: a = 8.3961(16) Å, b = 13.253(3) Å, and c = 13.510(3) Å, with cell angles of α = 72.953(7)°, β = 78.176(7)°, and γ = 72.835(7)°.

Figure 3a shows a monolayer cutout of **CP3**, demonstrating the planarity of the linker molecules arranged in two-dimensional sheets. These linker sheets are connected to each other through the bpe pillars, as depicted in Figure 3b, forming an angle of 73.3° between the pillars and the linker sheet. This makes the composition Zn_{2n}(sbcd)(bpe)-$(DMAc)_{3n}(H_2O)$ obvious, and the single crystals were furthermore analyzed with PXRD, TGA, and IR, confirming the successful incorporation of the linker and confirming the composition (Figures S4−S6). Induced by the angle, the distance between the pillar's connected layers is 13.4 Å. The SBU consists of two zinc cations connected by two bridging κ^1:κ^1 carboxylic (O1, O3) acid groups. Furthermore, two additional carboxylic acids (O2) bind in a κ^1 fashion, resulting in a total of four linker molecules connected to the metal node. Each zinc metal center is bound to a nitrogen atom (N1) from the bpe pillar, completing the tetrahedral coordination sphere of each zinc.

CP3 shows a 3-fold interpenetrated structure, leading to a close packing of the sbcd chromophores with a chromophore density of 1.22 mol/dm^3, similar to that of **CP2** (see Figure 3e). Comparably to **CP1** and **CP2**, the linkers are packed in off-center parallel stacking. However, in this case, the carbazoles of two sheets are aligned coplanar to each other at a distance of 3.50 Å, followed by a stilbene core of a third sheet stacked 3.99 Å above the carbazoles (Figure 3c) but now shifted by a larger margin of 2.50 Å compared to the previous CPs (Figure 3d). Additionally, there is a 57.5° rotation of the stilbene core compared with the carbazole.

In contrast to **CP2**, in **CP3**, the nuclearity of the zinc SBU, as well as the general structure of the pristine sheet like in **CP1** are preserved. However, compared to **CP1**, the bpe pillar can be imagined to be inserted in between the 2D "linker sheets", now connecting them by virtually replacing the originally coordinating water molecule of the Zn_2O_8 SBU, leading to $Zn_2N_2O_6$ SBUs and a three-dimensional network.

Despite the differences discussed in the structural arrangements induced by pillar incorporation, the tight packing and interpenetration resulted in comparable arrangements and observable interchromophoric distances within the three frameworks. However, a less distorted, i.e., more planar, molecular structure of the chromophore linkers is present both

https://doi.org/10.1021/acsaom.4c00080
ACS Appl. Opt. Mater. 2024, 2, 1770−1779

in **CP2** and **CP3** compared to **CP1**, this phenomenon is expected to positively influence 2PA.[9]

Steady-State Spectroscopy of H_4sbcd and CPs

The purity of the bulk material samples for photophysical characterization was confirmed by a combination of PXRD, TGA, and elemental analysis (Supporting Information). One-photon optical spectroscopy and IR spectroscopy (Figure S5) were performed for the H_4sbcd linker and corresponding CPs (Figure 4). H_4sbcd was dissolved in DMF with a concentration

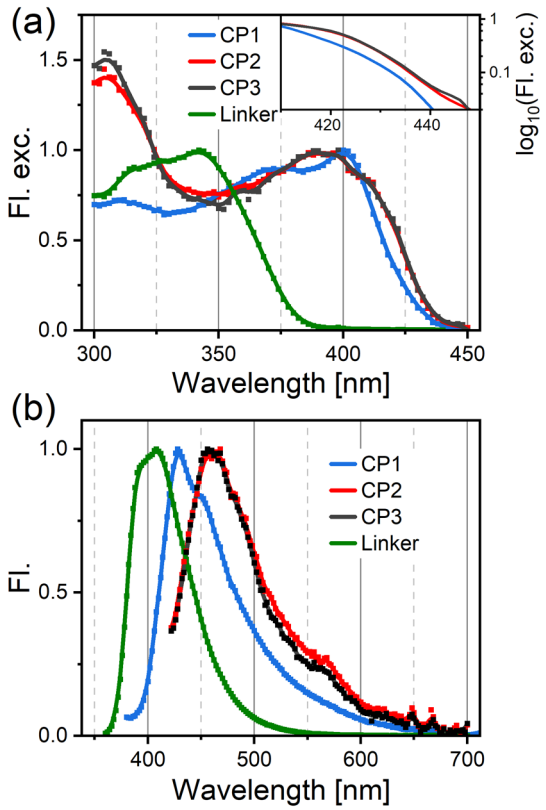

Figure 4. (a) Fluorescence excitation spectra of the H_4sbcd linker (detection wavelength at 450 nm) in DMF and corresponding CPs in the PMMA-film state. (b) Emission spectra of the H_4sbcd linker (excitation at 350 nm) and CPs. Note: to remove Raman peaks in the excitation and emission spectra for solid samples, CPs were excited and monitored at different wavelengths. For the excitation spectra of CPs, the detection wavelengths were set at 500, 510, and 520 nm, while for the emission spectra of CPs, the excitation wavelengths were set at 330, 340, 350, and 360 nm. Raman peaks can thus be removed significantly by stacking these excitation or emission spectra together.

of 10 μmol/L while solid samples of **CP1**, **CP2**, and **CP3** were prepared as a PMMA film using the doctor blade method with a concentration in the range of 9−38 mmol/L (see Table S3).

The excitation spectrum of the linker shows a broad absorption band at around 325 nm (Figure 4a). In comparison, the excitation spectra of the CPs show a redshift of approximately 50 nm and broadening in all CPs. The redshift, as well as the broadening of the absorption bands, points toward a higher excitonic interaction in the materials than in the linker.[26] In addition, structure rigidification and interligand charge transfer were also proposed to explain the spectral shift in the CP environment.[33−36] Comparing the CP-spectra, **CP1** shows the least pronounced redshift, while **CP2** and **CP3** are similar in this respect. The linear−log plot shown as an inset in Figure 4a shows that **CP3** extends marginally further to the red compared to CP2. A comparison of the CPs' emission spectra with the linker molecule again shows a redshift upon incorporation of the linker into the CPs. **CP1** shows a redshift of 25 nm, while **CP2** and **CP3** show similar emission spectra but are red-shifted up to 60 nm, as shown in Figure 4b. We note that the small emission peaks at wavelengths longer than 650 nm in the emission spectra of **CP2** and **CP3** originate from Raman scattering. The redshift in emission of the CPs compared to the linker can be rationalized by two structural effects. First, the $\pi-\pi$ interactions between adjacent linker molecules in the solid state may facilitate efficient intermolecular interactions through π-stacking.[37] Second, the increased planarity of the linker in **CP2** and **CP3** as compared to **CP1** may maximize the intramolecular π-orbital overlap and promote further $\pi-\pi$ interactions,[38] explaining the extra shift of the emission band.[38,39] Fluorescence quantum yields (QY) of all CPs are lower than those for the H_4sbcd linker in solution (Φ = 0.76). **CP1** shows the highest quantum yield Φ = 0.11, followed by **CP3** Φ = 0.015, and the lowest in **CP2** Φ = 0.010. Such a reduction of QY after incorporation of chromophores into the CP has been observed before and was explained by introduction of radiationless decay pathways by the pillars, aggregation, or reduction of the active H_4sbcd molecule in the pillar-layered CPs.[30] This, however, does not necessarily imply a lower $\sigma^{(2)}$ for the CPs, as a previous study inferred no direct correlation between the two values.[28]

Nonlinear Optical Characterization of the Linker and CPs

Nonlinear optical characterization of the linker and CPs was conducted via nonlinear Fourier-transform spectroscopy.[40] This method provides a broadband two-photon excitation spectrum for the substance under investigation. The used setup shares the working principle with the experiment of Hashimoto et al.,[40] with the exception that our design employs a noncollinear optical parametric amplifier (NOPA) for a broadband excitation laser and a common-path birefringent interferometer instead of a Michelson interferometer to generate pulse pairs. Pulse compression was achieved using a prism pair compressor, producing a routinely available 10 fs pulse for the 2PA measurement. The typical NOPA output falls in the range of 750−950 nm, tunable to shorter wavelengths if necessary. In this study, we utilized two NOPA spectral ranges to investigate the H_4sbcd linker and corresponding CPs, presenting the 2PA data in the fundamental wavelength range from 740 to 920 nm. $\sigma^{(2)}$ values were calibrated using fluorescein in water (pH 11) for the H_4sbcd linker and **CP1** for **CP2** and **CP3** (cf. Supporting Information).[26,41]

The 2PA spectrum of H_4sbcd is presented in Figure 5a. The 1PA spectrum shows an absorption edge at around 400 nm. This explains the lack of observable 2PA at a fundamental wavelength above 800 nm. Notably, $\sigma^{(2)}$ values are less than 3 GM in this region, emphasizing the sensitivity of our 2PA measurement technique. As the frequency-doubled fundamental wavelength begins to overlap with the 1PA spectrum, a sharp increase in $\sigma^{(2)}$ is observed, reaching up to 80 GM at 740 nm. It is anticipated that the $\sigma^{(2)}$ value for H_4sbcd will be even higher at shorter wavelengths, given the 1PA absorption band's peak intensity at 340 nm. Similar molecules featuring a stilbene core with carbazole donors have been previously studied for their 2PA cross-section, achieving values of up to 200 GM at 680 nm.[42]

https://doi.org/10.1021/acsaom.4c00080
ACS Appl. Opt. Mater. 2024, 2, 1770−1779

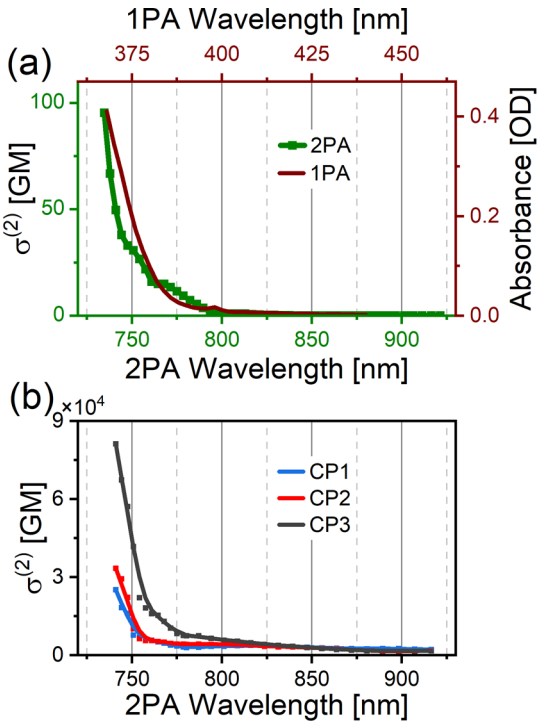

Figure 5. (a) Experimental 2PA spectrum of H_4sbcd in DMF (green dots and line) compared with its one-photon excitation spectrum (brown line). (b) 2PA spectra of **CP1** (blue), **CP2** (red), and **CP3** (dark gray).

After incorporating the linker molecules into CPs, the observed red-shift in the 1PA spectrum enables the measurement of 2PA from a wavelength of 900 nm, as depicted in Figure 5b. Within the employed excitation range, **CP2** exhibits $\sigma^{(2)}$ values ranging from 1340 to 33 457 GM, **CP3** values from 1501 to 81 267 GM, and **CP1** values from 2258 to 25 156 GM (Table 1). At this point, it should be noted that the $\sigma^{(2)}$ of **CP1**

Table 1. 2PA Cross-Sections of the Reported CPs/MOFs in the Range of 740 to 920 nm

CPs/MOFs	2PA cross-section $\sigma^{(2)}$ (10^3 GM)
Zn_{2n}(sbcd)$(DMAc)_{2n}(H_2O)_{1.5n}$ (**CP1**)	2.258−25.156
Zn_{2n}(sbcd)(bpy)$(DMAc)_{2n}(H_2O)_{3n}$ (**CP2**)	1.340−33.457
Zn_{2n}(sbcd)(bpe)$(DMAc)_{3n}(H_2O)$ (**CP3**)	1.501−81.267

deviates from our previous publication, which was measured using a fully automated Z-scan setup and showed values of 2137−15 838 GM.[26,43] We place greater confidence in the present data set due to the significantly extended data acquisition time required for Z-scan measurements in comparison to the interferometric approach outlined herein. Swept laser sources are often used in a Z-scan method; therefore, excitation intensities and pulse durations at each central wavelength must be characterized with great care. As a wavelength scanning method, recording a broadband 2PA spectrum may take several tens of minutes.[42,44,45] Consequently, the potential for sample degradation is more pronounced in the Z-scan measurement, impacting the result of the measurement.[46] As a contrast, in our approach, a broadband laser with 10 fs pulses was focused on the sample. Therefore, a complete 2PA spectrum can be acquired in less than 3 min.

In all cases, the generally enhanced 2PA of the CPs compared to that of the linker is attributed to the linker incorporation into the framework, as was observed in other cases.[9] Interestingly, with the same linker and SBU metal shared, the activity of the CPs varies significantly.

The 2PA cross-section of **CP1** and **CP2** stays relatively constant with a slight improvement in **CP2**, while **CP3** shows a drastically improved performance despite the fact that the observable packing of the linker stays similar with only minor differences. The enhancement of $\sigma^{(2)}$ in **CP2** and **CP3** with respect to **CP1** can be attributed to the planarization of the linker molecule.[47] This planarization, coupled with relatively short distances between chromophores in the material, likely results in stronger $\pi-\pi$ intermolecular interactions, known to positively influence the MPA response.[25,47] The different SBUs and sheet structures, however, appear not to have a big impact on the 2PA activity.

The 2.4-fold increase in $\sigma^{(2)}$ from **CP2** to **CP3** cannot be accounted for by the planarization of the linker in this comparison, as in both cases the linker remains planar. Notably, the rotation of the stilbene compared to the carbazole is smaller in **CP3** compared to that of **CP2** (57.5° vs 58.9°). This subtle difference may enhance intermolecular interactions, given that the stilbene is more in-plane with the carbazole, increasing orbital overlap and therefore increasing the charge-transfer between chromophores.[48] Furthermore, as illustrated in Figure 2e and 3d, the chromophore alignment in **CP3** is more coplanar than that in **CP2**. This is potentially amplifying intermolecular interactions and, consequently, the 2PA cross-section.[38] Moreover, the 3D-MOF structure in **CP3** enforces more rigidity compared to the 2D structures in **CP2** and **CP1**, likely contributing to the increased 2PA activity as well.[16]

Besides optimization of the structure to enhance the intermolecular interactions and rigidity in the CPs and, in turn, $\sigma^{(2)}$, this surprisingly large increase of $\sigma^{(2)}$ can be further rationalized by fine-tuning of nonresonant levels of centrosymmetric linkers in the CPs, as detailed in the following. Both the one-photon allowed states (with transitions shown in Figure 4a) and the nonresonant intermediate states (e in eq 2) follow the same selection rules and tend to behave similarly in terms of bathochromic shifts.[49] The same is not necessarily true for the two-photon active f' state. In fact, for centrosymmetric molecules such as stilbene—the parent compound of H_4sbcd—the rule of mutual exclusion applies for $g \rightarrow f$ and $g \rightarrow f'$ transitions. Accordingly, the one-photon resonance shifts between the linker and CPs (and between CPs), and the main peak for the two-photon resonance remains located at the blue edge of the excitation spectrum for the linker and all CPs, as depicted in Figure 5a. Assuming similar trends for the one-photon $g \rightarrow f$ transitions and the first step of a two-photon absorption process, $g \rightarrow e$, we can expect that frequency shift in the one-photon spectrum may indicate a shift in energy in the manifold of nonresonant e states. This situation is depicted in Figure 6. We note that the arguments made here apply rigorously to a generalized centrosymmetric system. More specific arguments would require quantitative quantum chemical calculations of 2PA cross sections of the free ligand and the ligand in the CP environment and are beyond the scope of this manuscript.[12]

https://doi.org/10.1021/acsaom.4c00080
ACS Appl. Opt. Mater. 2024, 2, 1770−1779

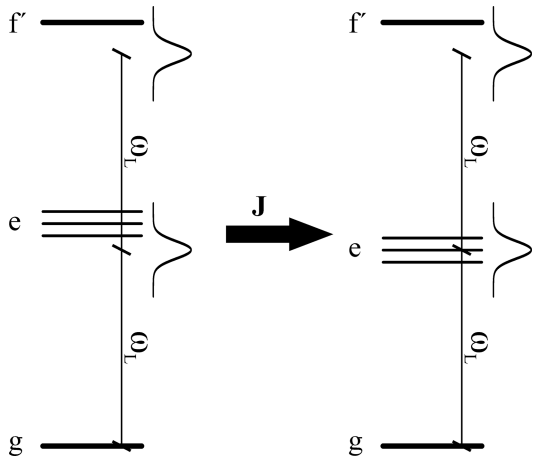

Figure 6. Schematic energy level diagram of a two-photon absorption process with a nonresonant intermediate step. For the uncoupled molecule (i.e., the linker, left side), the manifold on nonresonant states e is detuned from the laser frequency ω_L, contributing to 2PA decreasingly with detuning, see eq 2. The bandwidth of the exciting laser pulse is shown as a Gaussian curve. Upon coupling between chromophores with strength J, i.e., after incorporation of the linker into a CP, the e-manifold shifts toward the laser's center frequency ω_L, leading to increased 2PA. The two-photon state f' is unaffected by coupling.

The uncoupled molecule is assumed to have the energy level diagram shown on the left side of Figure 6. In this scenario, the e-manifold is detuned for laser frequency ω_L, making the $g \rightarrow e$ transition inefficient. This can be the scenario for the isolated linker molecule, explaining its moderate $\sigma^{(2)}$ values. Upon coupling (right side of Figure 6), we expect the e-manifold to red-shift, following the trend of the one-photon absorption spectrum. Even a marginal red-shift may bring the e-manifold in resonance with ω_L. This has no effect on the 1PA cross-section (see Figure 4) but leads to potentially drastic changes in the 2PA cross-section as the denominator of eq 2 can approach zero. We note that changes in solvent polarizability were shown to have a strong effect on $\sigma^{(2)}$, which can, in analogy to the above argument, be interpreted as a shift of the e-manifold.[50]

In summary, there are several arguments based on chemistry and/or crystal structure to explain an increase in 2PA activity of a linker when inserted into a CP.[25] Briefly, the polar CP environment may lead to planarization of the linker or to an increase in charge-transfer character, which is readily associated with larger 2PA cross sections.[51] Similarly, the relative arrangement of transition dipole moments within a CP can lead to enhanced 2PA based on, e.g., excitonic effects.[11] This influence of transition dipole moments $\vec{\mu}$ on 2PA is readily seen in the numerator of eq 2. We add an argument based on the denominator of the said equation. Even a small change in transition frequencies ω_{eg} can lead to a drastic increase of 2PA if it brings ω_{eg} closer to the $\omega_{eg} = \omega_L$ resonance condition.

CONCLUSION

In conclusion, the synthesis and structural characterization of two new coordination polymers (CPs) based on the linker molecule 9,9′-stilbene-bis-carbazole-3,6-dicarboxylic acid (H_4sbcd) have been presented: a two-dimensional CP Zn_{2n}(sbcd)(bpy)$(DMAc)_{2n}(H_2O)_{3n}$ (**CP2**) and a three-dimensional metal−organic framework Zn_{2n}(sbcd)(bpe)-$(DMAc)_{3n}(H_2O)$ (**CP3**). Both structures were synthesized via a solvothermal approach adjusted from the synthesis of $Zn_{2n}(sbcd)(DMAc)_{2n}(H_2O)_{1.5n}$ **CP1** previously reported by our group,[26] additionally incorporating ditopic pillar molecules (bpy for **CP2** or bpe for **CP3**, respectively). The introduction of the pillars leads to distinct structural differences in the CP, either by virtual insertion into the dinuclear SBU (**CP2**) or by bridging of the pristine 2D periodic sheets (**CP3**) with reference to the original **CP1**. Both new CPs exhibited enhanced molecular planarity and reduced distortion in the sbcd linker structure. However, the packing of the linkers was only marginally affected compared to CP1.

In-depth photophysical characterization revealed bathochromic shifts in the excitation and emission spectra for all CPs compared to those of the free linker, possibly explained by enhanced excitonic interactions and $\pi-\pi$ interactions within the materials. The nonlinear optical characterization using 2PA spectroscopy demonstrated enhanced 2PA in the CPs compared to the free linker, with **CP3** exhibiting a remarkable 2.4-fold increase in $\sigma^{(2)}$ compared to **CP2** and 3.2-fold increase over **CP1**. The coplanar alignment of chromophores in **CP3**, along with its 3D structure, likely contributes to this increase, emphasizing the importance of structural considerations in influencing the 2PA activity. Accordingly, future CP design should target rigid 3D structures with closely packed chromophores to obtain a high 2PA activity. On a more general level, we find that fine-tuning nonresonant levels has the potential to strongly increase 2PA activity, for centrosymmetric linkers such as stilbene, the desired redshift of nonresonant levels is accompanied by a—maybe subtle—bathochromic shift of the one-photon absorption spectrum. This could be further probed by impedance spectroscopy to further study the influence of the polarization and dielectric constant of the MOFs on the nonresonant levels.[50,52]

The obtained pillar-layered CPs have the highest $\sigma^{(2)}$ among other pillared-layer CPs. The first synthesized pillar-layered CPs by Vittal et al. using the An2Py linker reached values of up to 32.7 GM.[16,28,31] Fischer and colleagues synthesized pillar-layered CPs using the MPA active linker tetra-(4-carboxylphenyl)ethylene (H_4TCPE), reaching values of up to 476 GM, and Vittal et al. improved on this with values up to 74 000 GM by changing the used pillars.[29,30] This competitive performance of pillar-layered systems shows the potential of carbazole-based chromophores in MPA active CPs and MOFs.

The findings show that the pillar-layering approach is a potent way to produce varied CP materials implementing the same chromophores and, in general, contributes to the broader field of CPs and their potential applications in nonlinear optical devices.

EXPERIMENTAL SECTION

Materials and Methods

All purchased reagents were received from chemical suppliers and used without any further purification unless otherwise stated. Dipropyl-9-(4-nitrophenyl)-carbazole-3,6-dicarboxylate and 9,9′-(stilbyl)-bis(carbazole-3,6-dicarboxylic acid) were synthesized following the previously published synthesis procedures.[26,53] All reactions with air- and moisture-sensitive compounds were carried out under standard Schlenk techniques using Argon 4.6 (Westfalen) or in a glovebox (UNIlab, M. Braun). Required glassware was flame-dried in vacuo prior to use. Elemental analysis was performed at the microanalytical laboratory at the Technical University of Munich.

https://doi.org/10.1021/acsaom.4c00080
ACS Appl. Opt. Mater. 2024, 2, 1770−1779

Analysis of C, H, and N values was conducted by using the flash combustion method at 1800 °C. NMR spectra were recorded on a Bruker AV400 instrument at room temperature at 400 MHz. Single-crystal X-ray diffraction (SC-XRD) data were collected on a Bruker D8 Venture system equipped with a Mo TXS rotating anode (λ = 0.71073 Å) and a CMOS photon 100 detector (for detailed information, see the Supporting Information). Capillary PXRD measurements were recorded in transmission geometry on a Stoe STADI P diffractometer equipped with Mo radiation (λ = 0.7093 Å), a curved Ge(111) monochromator, and a Dectris Mythen 1K detector. Fluorescence emission and excitation measurements were recorded on an FS5 spectrofluorometer from Edinburgh Instruments either in solution (linker) or in a PMMA matrix (CPs). For the PMMA matrix, all three CP crystalline powders are finely ground to uniform powders. Each CP powder was weighed and mixed with 0.5 g of PMMA (1.18 g/mL) powder in 5 mL of DCM and stirred for 2 h in the solution. Afterward, PMMA films of the resulting dispersions were produced by using the "doctor blading" technique with subsequent evaporation of the DCM. These samples were then used for 2PA measurements as well. IR measurements were conducted on a PerkinElmer Frontier FT-IR spectrometer. Quantum yield measurements in solution and the solid state were performed on a Hamamatsu Quantaurus-QY Absolute PL quantum yield spectrometer in the scan method in a range of 300−390 nm.

Synthesis

Zn_{2n}(sbcd)(bpy)$(DMAc)_{2n}(H_2O)_{3n}$. In a 4 mL scintillation vial, 10.0 mg of H_4sbcd (14.7 μmol, 1.0 equiv) dissolved in 1 mL of DMAc, 5.68 mg of 4,4′-bipyridine (36.4 μmol, 2.5 equiv) dissolved in 1 mL of DMAc, and 13.0 mg of $Zn(NO_3)_2{\cdot}6H_2O$ dissolved in 0.5 mL of H_2O are added subsequently and heated for 2 days at 90 °C. The resulting white crystalline precipitate is filtered off, washed with DMAc, and dried under air. 8.02 mg (10.4 μmol, 69%) of a white crystalline powder is obtained. EA calcd. for $Zn_2C_{52}H_{30}N_4O_8{\cdot}2C_4H_9O{\cdot}3H_2O$: C, 60.16; H, 4.54; N, 7.02. Found: C, 59.41; H, 4.47; N, 6.66.

Zn_{2n}(sbcd)(bpe)$(DMAc)_{3n}(H_2O)$. 13.0 mg of $Zn(NO_3)_2{\cdot}6H_2O$ is put into a 4 mL scintillation vial. Subsequently, 10.0 mg of H_4sbcd (14.7 μmol, 1.0 equiv) and 6.70 mg of bpe (36.4 μmol, 2.5 equiv) are dissolved in, respectively, 1 mL of DMAc and added to the metal salts. The solution is heated to 90 °C in an oven for 2 days. The obtained white precipitate is filtered off, washed with DMAc, and dried. This yields 5.71 mg (8.94 μmol, 61%) of a light-yellow crystalline powder. EA calcd. for $Zn_2C_{54}H_{34}N_4O_8{\cdot}3C_4H_9O{\cdot}H_2O$: C, 62.08; H, 4.97; N, 7.68. Found: C, 61.27; H, 4.66; N, 7.51.

■ ASSOCIATED CONTENT

Supporting Information

The Supporting Information is available free of charge at https://pubs.acs.org/doi/10.1021/acsaom.4c00080.

Additional synthetic procedures; NMR spectra; IR, PXRD, and TGA; two-photon absorption data processing; and single-crystal X-ray data (PDF)

Accession Codes

CCDC 2333064−2333065 contains the supplementary crystallographic data for this paper. These data can be obtained free of charge via www.ccdc.cam.ac.uk/data_request/cif, or by emailing data_request@ccdc.cam.ac.uk, or by contacting The Cambridge Crystallographic Data Centre, 12 UnionRoad, Cambridge CB2 1EZ, U.K.; fax: + 44 1223 336033.

■ AUTHOR INFORMATION

Corresponding Authors

Jürgen Hauer − *Technical University of Munich, TUM School of Natural Sciences, Department of Chemistry, Professorship for Dynamic Spectroscopy, Catalysis Research Center, 85747 Garching, Germany*; Email: juergen.hauer@tum.de

Alexander Pöthig − *Technical University of Munich, TUM School of Natural Sciences, Department of Chemistry, Chair of Inorganic and Metal−Organic Chemistry, Catalysis Research Center, 85747 Garching, Germany*; orcid.org/0000-0003-4663-3949; Email: alexander.poethig@tum.de

Authors

Simon N. Deger − *Technical University of Munich, TUM School of Natural Sciences, Department of Chemistry, Chair of Inorganic and Metal−Organic Chemistry, Catalysis Research Center, 85747 Garching, Germany*

Yang Cui − *Technical University of Munich, TUM School of Natural Sciences, Department of Chemistry, Professorship for Dynamic Spectroscopy, Catalysis Research Center and TUM School of Natural Sciences, Department of Physics, Catalysis Research Center, 85747 Garching, Germany*; orcid.org/0000-0003-2116-7611

Julien Warnan − *Technical University of Munich, TUM School of Natural Sciences, Department of Chemistry, Chair of Inorganic and Metal−Organic Chemistry, Catalysis Research Center, 85747 Garching, Germany*; orcid.org/0000-0003-2729-8997

Roland A. Fischer − *Technical University of Munich, TUM School of Natural Sciences, Department of Chemistry, Chair of Inorganic and Metal−Organic Chemistry, Catalysis Research Center, 85747 Garching, Germany*; orcid.org/0000-0002-7532-5286

František Šanda − *Institute of Physics, Faculty of Mathematics and Physics, Charles University, Prague 121 16, Czech Republic*; orcid.org/0000-0003-2416-8804

Complete contact information is available at: https://pubs.acs.org/10.1021/acsaom.4c00080

Author Contributions

⊥S.N.D. and Y.C. contributed equally to this work. S.N.D.: conceptualization, methodology, validation, formal analysis, investigation, data curation, writing—original draft, review and editing, visualization. Y.C.: methodology, validation, formal analysis, investigation, data curation, writing—original draft, review and editing, visualization. J.W.: supervision, writing—review and editing. F.S.: writing—review and editing. R.A.F.: resources, writing—review and editing, supervision, project administration. J.H. conceptualization, supervision, writing—review and editing, resources, project administration. A.P. conceptualization, supervision, writing—review and editing, resources, project administration.

Funding

The authors would like to thank the German Research Foundation (DFG) for funding within the frame of the EXC 2089 Cluster of Excellence and the Priority Programme "COORNETs" (SPP 1928). F.S. is supported by the Czech Science Foundation (GACR) through grant no. 22-26376S.

Notes

The authors declare no competing financial interest.

■ ACKNOWLEDGMENTS

The authors would like to thank the German Research Foundation (DFG) for funding within the frame of the EXC 2089 Cluster of Excellence and the Priority Programme

"COORNETs" (SPP 1928). The TUM is greatly acknowledged for its institutional funding. S.N.D. and Y.C. would like to thank the TUM Graduate School for financial support. S.N.D. would like to thank Silva Kronawitter for the support with measurements.

REFERENCES

(1) Moulton, P. F.; Rines, G. A.; Slobodtchikov, E. V.; Wall, K. F.; Frith, G.; Samson, B.; Carter, A. L. G. Tm-Doped Fiber Lasers: Fundamentals and Power Scaling. *IEEE J. Sel. Top. Quantum Electron.* **2009**, *15* (1), 85−92.
(2) Monguzzi, A.; Tubino, R.; Hoseinkhani, S.; Campione, M.; Meinardi, F. Low power, non-coherent sensitized photon up-conversion: modelling and perspectives. *Phys. Chem. Chem. Phys.* **2012**, *14* (13), 4322−4332.
(3) Byer, R. L. Nonlinear Optical Phenomena and Materials. *Annu. Rev. Mater. Sci.* **1974**, *4* (1), 147−190.
(4) Chen, W. Spatial nonlinear optics for securing information. *Light Sci. Appl.* **2022**, *11* (1), 11.
(5) Dini, D.; Calvete, M. J. F.; Hanack, M. Nonlinear Optical Materials for the Smart Filtering of Optical Radiation. *Chem. Rev.* **2016**, *116* (22), 13043−13233.
(6) Wei, Z.; Pan, Y.; Hou, G.; Ran, X.; Chi, Z.; He, Y.; Kuang, Y.; Wang, X.; Liu, R.; Guo, L. Excellent Multiphoton Excitation Fluorescence with Large Multiphoton Absorption Cross Sections of Arginine-Modified Gold Nanoclusters for Bioimaging. *ACS Appl. Mater. Interfaces* **2022**, *14* (2), 2452−2463.
(7) Bhawalkar, J. D.; He, G. S.; Prasad, P. N. Nonlinear multiphoton processes in organic and polymeric materials. *Rep. Prog. Phys.* **1996**, *59* (9), 1041.
(8) He, G. S.; Tan, L.-S.; Zheng, Q.; Prasad, P. N. Multiphoton Absorbing Materials: Molecular Designs, Characterizations, and Applications. *Chem. Rev.* **2008**, *108* (4), 1245−1330.
(9) Medishetty, R.; Zaręba, J. K.; Mayer, D.; Samoć, M.; Fischer, R. A. Nonlinear optical properties, upconversion and lasing in metal−organic frameworks. *Chem. Soc. Rev.* **2017**, *46* (16), 4976−5004.
(10) Pawlicki, M.; Collins, H. A.; Denning, R. G.; Anderson, H. L. Two-Photon Absorption and the Design of Two-Photon Dyes. *Angew. Chem., Int. Ed.* **2009**, *48* (18), 3244−3266.
(11) Weishäupl, S. J.; Mayer, D. C.; Cui, Y.; Kumar, P.; Oberhofer, H.; Fischer, R. A.; Hauer, J.; Pöthig, A. Recent advances of multiphoton absorption in metal−organic frameworks. *J. Mater. Chem. C* **2022**, *10* (18), 6912−6934.
(12) Ohta, K.; Antonov, L.; Yamada, S.; Kamada, K. Theoretical study of the two-photon absorption properties of several asymmetrically substituted stilbenoid molecules. *J. Chem. Phys.* **2007**, *127* (8), No. 084504.
(13) Walters, G.; Sutherland, B. R.; Hoogland, S.; Shi, D.; Comin, R.; Sellan, D. P.; Bakr, O. M.; Sargent, E. H. Two-Photon Absorption in Organometallic Bromide Perovskites. *ACS Nano* **2015**, *9* (9), 9340−9346.
(14) Nalwa, H. S. Organic Materials for Third-Order Nonlinear Optics. *Adv. Mater.* **1993**, *5* (5), 341−358.
(15) Terenziani, F.; Katan, C.; Badaeva, E.; Tretiak, S.; Blanchard-Desce, M. Enhanced Two-Photon Absorption of Organic Chromophores: Theoretical and Experimental Assessments. *Adv. Mater.* **2008**, *20* (24), 4641−4678.
(16) Quah, H. S.; Chen, W.; Schreyer, M. K.; Yang, H.; Wong, M. W.; Ji, W.; Vittal, J. J. Multiphoton harvesting metal−organic frameworks. *Nat. Commun.* **2015**, *6* (1), 7954.
(17) Kirchon, A.; Feng, L.; Drake, H. F.; Joseph, E. A.; Zhou, H.-C. From fundamentals to applications: a toolbox for robust and multifunctional MOF materials. *Chem. Soc. Rev.* **2018**, *47* (23), 8611−8638.
(18) Stanley, P. M.; Su, A. Y.; Ramm, V.; Fink, P.; Kimna, C.; Lieleg, O.; Elsner, M.; Lercher, J. A.; Rieger, B.; Warnan, J.; Fischer, R. A. Photocatalytic CO2-to-Syngas Evolution with Molecular Catalyst Metal-Organic Framework Nanozymes. *Adv. Mater.* **2023**, *35* (6), No. 2207380.
(19) Connolly, B. M.; Aragones-Anglada, M.; Gandara-Loe, J.; Danaf, N. A.; Lamb, D. C.; Mehta, J. P.; Vulpe, D.; Wuttke, S.; Silvestre-Albero, J.; Moghadam, P. Z.; Wheatley, A. E. H.; Fairen-Jimenez, D. Tuning porosity in macroscopic monolithic metal-organic frameworks for exceptional natural gas storage. *Nat. Commun.* **2019**, *10* (1), 2345.
(20) Medishetty, R.; Nemec, L.; Nalla, V.; Henke, S.; Samoć, M.; Reuter, K.; Fischer, R. A. Multi-Photon Absorption in Metal−Organic Frameworks. *Angew. Chem., Int. Ed.* **2017**, *56* (46), 14743−14748.
(21) Mingabudinova, L. R.; Vinogradov, V. V.; Milichko, V. A.; Hey-Hawkins, E.; Vinogradov, A. V. Metal−organic frameworks as competitive materials for non-linear optics. *Chem. Soc. Rev.* **2016**, *45* (19), 5408−5431.
(22) D'Aléo, A.; Felouat, A.; Heresanu, V.; Ranguis, A.; Chaudanson, D.; Karapetyan, A.; Giorgi, M.; Fages, F. Two-photon excited fluorescence of BF2 complexes of curcumin analogues: toward NIR-to-NIR fluorescent organic nanoparticles. *J. Mater. Chem. C* **2014**, *2* (26), 5208−5215.
(23) Johann, T.; Schmidt, K.; Prabhakaran, P.; Zentel, R.; Lee, K.-S. Two-photon absorption dye based on 2,5-bis(phenylacrylonitrile)-thiophene with aggregation enhanced fluorescence. *Opt. Mater. Express* **2016**, *6* (4), 1296−1305.
(24) Mei, J.; Leung, N. L. C.; Kwok, R. T. K.; Lam, J. W. Y.; Tang, B. Z. Aggregation-Induced Emission: Together We Shine, United We Soar! *Chem. Rev.* **2015**, *115* (21), 11718−11940.
(25) Mayer, D. C.; Manzi, A.; Medishetty, R.; Winkler, B.; Schneider, C.; Kieslich, G.; Pöthig, A.; Feldmann, J.; Fischer, R. A. Controlling Multiphoton Absorption Efficiency by Chromophore Packing in Metal−Organic Frameworks. *J. Am. Chem. Soc.* **2019**, *141* (29), 11594−11602.
(26) Weishäupl, S. J.; Cui, Y.; Deger, S. N.; Syed, H.; Ovsianikov, A.; Hauer, J.; Pöthig, A.; Fischer, R. A. Coordination Polymers Based on Carbazole-Derived Chromophore Linkers for Optimized Multiphoton Absorption: A Structural and Photophysical Study. *Chem. Mater.* **2022**, *34* (16), 7402−7411.
(27) ZareKarizi, F.; Joharian, M.; Morsali, A. Pillar-layered MOFs: functionality, interpenetration, flexibility and applications. *J. Mater. Chem. A* **2018**, *6* (40), 19288−19329.
(28) Quah, H. S.; Nalla, V.; Zheng, K.; Lee, C. A.; Liu, X.; Vittal, J. J. Tuning Two-Photon Absorption Cross Section in Metal Organic Frameworks. *Chem. Mater.* **2017**, *29* (17), 7424−7430.
(29) Mayer, D. C.; Zaręba, J. K.; Raudaschl-Sieber, G.; Pöthig, A.; Chołuj, M.; Zaleśny, R.; Samoć, M.; Fischer, R. A. Postsynthetic Framework Contraction Enhances the Two-Photon Absorption Properties of Pillar-Layered Metal−Organic Frameworks. *Chem. Mater.* **2020**, *32* (13), 5682−5690.
(30) Liu, N.; Chen, Z.; Fan, W.; Su, J.; Lin, T.; Xiao, S.; Meng, J.; He, J.; Vittal, J. J.; Jiang, J. Highly Efficient Multiphoton Absorption of Zinc-AIEgen Metal−Organic Frameworks. *Angew. Chem., Int. Ed.* **2022**, *61* (12), No. e202115205.
(31) Rath, B. B.; Kottilil, D.; Ji, W.; Vittal, J. J. Enhancement in Two-Photon Absorption and Photoluminescence in Single Crystals of Cd(II) Metal Organic Frameworks. *ACS Appl. Mater. Interfaces* **2023**, *15* (22), 26939−26945.
(32) Martinez, C. R.; Iverson, B. L. Rethinking the term "pi-stacking. *Chem. Sci.* **2012**, *3* (7), 2191−2201.
(33) Yao, Z.; Yang, L.; Cai, Y.; Yan, C.; Zhang, M.; Cai, N.; Dong, X.; Wang, P. Rigidifying the π-Linker to Enhance Light Absorption of Organic Dye-Sensitized Solar Cells and Influences on Charge Transfer Dynamics. *J. Phys. Chem. C* **2014**, *118* (6), 2977−2986.
(34) Huang, H.; Yang, L.; Facchetti, A.; Marks, T. J. Organic and Polymeric Semiconductors Enhanced by Noncovalent Conformational Locks. *Chem. Rev.* **2017**, *117* (15), 10291−10318.
(35) McCarthy, B. D.; Hontz, E. R.; Yost, S. R.; Van Voorhis, T.; Dincă, M. Charge Transfer or J-Coupling? Assignment of an Unexpected Red-Shifted Absorption Band in a Naphthalenediimide-

https://doi.org/10.1021/acsaom.4c00080
ACS Appl. Opt. Mater. 2024, 2, 1770−1779

Based Metal−Organic Framework. *J. Phys. Chem. Lett.* **2013**, *4* (3), 453−458.
(36) Yang, L.; Yu, Y.; Feng, J.; Wu, J.; Jiang, L.; Dan, Y.; Qiu, Y. Charge transfer induced unexpected red-shift absorption of Zn and Cu porous coordination polymers based on electron-withdrawing ligand. *J. Photochem. Photobiol., A* **2018**, *350*, 103−110.
(37) Vaganova, T. A.; Gatilov, Y. V.; Benassi, E.; Chuikov, I. P.; Pishchur, D. P.; Malykhin, E. V. Impact of molecular packing rearrangement on solid-state fluorescence: polyhalogenated N-hetarylamines vs. their co-crystals with 18-crown-6. *CrystEngComm* **2019**, *21* (39), 5931−5946.
(38) Che, Y.; Perepichka, D. F. Quantifying Planarity in the Design of Organic Electronic Materials. *Angew. Chem., Int. Ed.* **2021**, *60* (3), 1364−1373.
(39) Bauer, C. A.; Timofeeva, T. V.; Settersten, T. B.; Patterson, B. D.; Liu, V. H.; Simmons, B. A.; Allendorf, M. D. Influence of Connectivity and Porosity on Ligand-Based Luminescence in Zinc Metal−Organic Frameworks. *J. Am. Chem. Soc.* **2007**, *129* (22), 7136−7144.
(40) Hashimoto, H.; Isobe, K.; Suda, A.; Kannari, F.; Kawano, H.; Mizuno, H.; Miyawaki, A.; Midorikawa, K. Measurement of two-photon excitation spectra of fluorescent proteins with nonlinear Fourier-transform spectroscopy. *Appl. Opt.* **2010**, *49* (17), 3323−3329.
(41) Makarov, N. S.; Drobizhev, M.; Rebane, A. Two-photon absorption standards in the 550−1600 nm excitation wavelength range. *Opt. Express* **2008**, *16* (6), 4029−4047.
(42) Segal, J.; Kotler, Z.; Sigalov, M.; Ben-Asuly, A.; Khodorkovsky, V. *Two-Photon Absorption Properties of (N-carbazolyl)-Stilbenes*; SPIE, 1999.
(43) Steiger, W.; Gruber, P.; Theiner, D.; Dobos, A.; Lunzer, M.; Van Hoorick, J.; Van Vlierberghe, S.; Liska, R.; Ovsianikov, A. Fully automated z-scan setup based on a tunable fs-oscillator. *Opt. Mater. Express* **2019**, *9* (9), 3567−3581.
(44) Ajami, A.; Husinsky, W.; Ovsianikov, A.; Liska, R. Dispersive white light continuum single Z-scan for rapid determination of degenerate two-photon absorption spectra. *Appl. Phys. B: Laser Opt.* **2018**, *124* (7), 142.
(45) Rumi, M.; Perry, J. W. Two-photon absorption: an overview of measurements and principles. *Adv. Opt. Photon.* **2010**, *2* (4), 451−518.
(46) Nag, A.; De, A. K.; Goswami, D. Two-photon cross-section measurements using an optical chopper: z-scan and two-photon fluorescence schemes. *J. Phys. B* **2009**, *42* (6), No. 065103.
(47) Lee, S.; Thomas, K. R. J.; Thayumanavan, S.; Bardeen, C. J. Dependence of the Two-Photon Absorption Cross Section on the Conjugation of the Phenylacetylene Linker in Dipolar Donor−Bridge−Acceptor Chromophores. *J. Phys. Chem. A* **2005**, *109* (43), 9767−9774.
(48) Rajput, S. S.; Zaleśny, R.; Alam, M. M. Chromophore Planarity, − BH Bridge Effect, and Two-Photon Activity: Bi- and Ter-Phenyl Derivatives as a Case Study. *J. Phys. Chem. A* **2023**, *127* (38), 7928−7936.
(49) Collins, J. Two-Photon Absorption and Applications to Biological Systems. In *Biophotonics: Spectroscopy, Imaging, Sensing, and Manipulation*; Springer: Dordrecht, The Netherlands, 2011; Bartolo, B. D., Collins, J., Eds.; pp 261−285.
(50) Wielgus, M.; Michalska, J.; Samoc, M.; Bartkowiak, W. Two-photon solvatochromism III: Experimental study of the solvent effects on two-photon absorption spectrum of p-nitroaniline. *Dyes Pigm.* **2015**, *113*, 426−434.
(51) Watanabe, S.; Tahara, A.; Isozaki, T.; Kinoshita, S.; Takeuchi, R.; Kashihara, W.; Suzuki, T. Effects of Two Electron-Donating and/or -Withdrawing Substituents on Two-Photon Absorption for Diphenylacetylene Derivatives. *J. Phys. Chem. A* **2023**, *127* (30), 6204−6212.
(52) Sorbara, S.; Mukherjee, S.; Schneemann, A.; Fischer, R. A.; Macchi, P. Hydrophobicity and dielectric properties across an isostructural family of MOFs: a duet or a duel? *ChemComm* **2022**, *58* (92), 12823−12826.
(53) Weishäupl, S. J.; Mayer, D. C.; Thyrhaug, E.; Hauer, J.; Pöthig, A.; Fischer, R. A. A nitrophenyl-carbazole based push-pull linker as a building block for non-linear optical active coordination polymers: A structural and photophysical study. *Dyes Pigm.* **2021**, *186*, No. 109012.

https://doi.org/10.1021/acsaom.4c00080
ACS Appl. Opt. Mater. 2024, 2, 1770−1779